Science and Technology Indonesia
e-ISSN:2580-4391 *p*-ISSN:2580-4405
Vol. 11, No. 3, July 2026

Research Paper

Synergistic Integration of Multi-Sensor Satellite Data and Gradient Boosting Machine Learning for High-Resolution $PM_{2.5}$ Estimation during Tropical Peatland Fires

Dessy Gusnita[1], Iis Sofiati[1], Fadhlullah Ramadhani[3], Angga Yolanda Putra[2], Risyanto[1], Waluyo Eko Cahyono[1], Tatik Kartika[3], Muhammad Priyatna[3]*, Estiningtyas Kusumastuti[4]

[1]*Research Center for Climate and Atmosphere, National Research and Innovation Agency, Bandung, West Java, 40135, Indonesia*
[2]*Directorate of Laboratory Management, Research Facilities, and Science and Technology Park, National Research and Innovation Agency, Jakarta, 10340, Indonesia*
[3]*Research Center for Geoinformatics, National Research and Innovation Agency, Bogor, West Java, 16911, Indonesia*
[4]*Environment Agency of Pontianak City, Pontianak, West Kalimantan, 78113, Indonesia*
***Corresponding author**: muha054@brin.go.id

Abstract

Tropical peatland and forest fires are critical contributors to regional haze and public health crises, yet ground-based monitoring in these regions remains sparse. This study develops a robust framework for estimating surface $PM_{2.5}$ concentrations during extreme fire events (2021–2025) by integrating multi-sensor satellite observations with in-situ data through a Hist Gradient Boosting Regressor (HGBR) approach. To enhance predictive accuracy, we implemented advanced feature engineering, including 1–3 days of exogenous lags, rolling statistics (3 and 7-day windows), and aerosol–meteorological interaction variables. Our analysis of multiple pollutants ($PM_{2.5}$, NO_2, SO_2, CO, HC, and O_3) reveals that during active fire periods, the Air Quality Index (AQI) frequently escalated to "Unhealthy" and "Hazardous" levels. The proposed HGBR model demonstrated high fidelity in representing spatiotemporal variability, achieving a coefficient of determination (R^2 = 0.72), with an RMSE of 14.26 $\mu g/m^3$ and MAE of 8.49 $\mu g/m^3$ (n = 339). These results validate the efficacy of machine learning-driven satellite monitoring in bypassing the limitations of fragmented ground station networks. This framework offers a scalable solution for operational air quality forecasting and early warning systems in fire-prone equatorial regions.

Keywords

Machine Learning, $PM_{2.5}$ Estimation, Histogram-Based Gradient Boosting, Tropical Peatland Fires, Multi-Sensor Satellite, Air Quality Dynamics

Received: 18 March 2026, Accepted: 27 May 2026
https://doi.org/10.26554/sti.2026.11.3.1089-1105

1. INTRODUCTION

The city of Pontianak, located in West Kalimantan and surrounded by vast tropical peatlands, is highly vulnerable to seasonal forest and land fires. During the dry season, the synergy between rainfall deficits, low humidity, and high temperatures triggers intense fire episodes. Regional wind patterns further exacerbate this by transporting smoke across administrative boundaries, causing hazardous air quality even when fire sources are distant (Marlier et al., 2015; Van Der Werf et al., 2017). Despite these recurring crises, ground-based monitoring in secondary cities like Pontianak remains spatially sparse, restricting the ability to capture intra-urban variability and rapid pollution spikes. This creates a critical gap in understanding air quality dynamics in fire-prone equatorial urban environments. Fine particulate matter ($PM_{2.5}$) is the primary pollutant from biomass burning, significantly increasing risks of respiratory and cardiovascular diseases (Burnett et al., 2018; Johnston et al., 2012; Murray et al., 2020; Pope and Dockery, 2006). Beyond $PM_{2.5}$, fires release gaseous precursors such as NO_2, CO, SO_2, and O_3, which synergistically degrade public health (Crippa et al., 2016; Reid et al., 2013). Since satellite sensors do not measure surface concentrations directly but observe proxies like Aerosol Optical Depth (AOD) and fire radiative power, a robust modelling framework is required to harmonize these multi-sensor data sources.

Google Earth Engine (GEE) has emerged as a transformative platform for such high-resolution spatiotemporal analysis (Velastegui-Montoya et al., 2023; Zhao et al., 2021). By providing cloud-based access to MODIS, VIIRS, Sentinel-5P, and ERA5 reanalysis data, GEE enables reproducible air quality tracking without intensive local computing infrastructure. While recent studies have utilized GEE for $PM_{2.5}$ estimation (Arshad et al., 2025; Miah et al., 2025), many remain focused on large metropolitan areas or limited temporal scales. Urban-scale assessments in secondary cities under multi-year variability remain insufficiently explored.

To address these limitations, this study develops a multi-sensor $PM_{2.5}$ estimation framework using the Hist Gradient Boosting Regressor (HGBR) within GEE for the 2021–2025 period. Unlike traditional regression or static models, our approach incorporates advanced temporal feature engineering, including 1-3 day exogenous lags, rolling statistics, and aerosol-meteorological interaction terms. These features are critical for capturing both immediate and delayed atmospheric responses during peat fire events (Ghafarian et al., 2022). Specifically, this research aims to: (1) analyse in-situ air quality trends in Pontianak, (2) estimate surface $PM_{2.5}$ using integrated satellite data, and (3) evaluate model performance against ground observations across varying fire intensities. This framework offers a scalable, cost-effective solution for operational air quality forecasting and haze mitigation in Indonesia's fire-prone regions.

2. EXPERIMENTAL SECTION

2.1 Data Sources and Integration

This study integrates high-resolution in-situ monitoring with multi-sensor satellite observations to characterize air quality dynamics in Pontianak (2021–2025). Ground-based air pollution data, including $PM_{2.5}$, PM_{10}, NO_2, CO, SO_2, O_3, and HC, were obtained from the Air Quality Monitoring System (AQMS) managed by the Pontianak Environment Agency. Corresponding meteorological parameters (rainfall, relative humidity, temperature, and wind vectors) were sourced from the Pontianak Observation Station, BRIN. To provide context on fire activity, hotspot data and burned area extents were integrated from the SIPONGI system (Ministry of Environment and Forestry).

Satellite-based air quality estimation and analysis require the integration of multi-sensor data capable of comprehensively representing atmospheric physical and chemical processes, particularly in tropical regions that are strongly affected by forest and land fires. No single satellite product can directly describe surface $PM_{2.5}$ dynamics, so the common approach is to combine information on aerosols, trace gas columns, meteorological variables, atmospheric boundary layer structure, and fire activity indicators.

Since no single satellite product directly measures surface $PM_{2.5}$, a multi-sensor framework was employed to represent atmospheric physical and chemical processes. Table 1 summarizes the satellite and reanalysis products used, covering aerosol properties, trace gas columns, and atmospheric boundary layer structure. Each variable was extracted using a station-based buffer approach and synchronized to a daily temporal scale. All data were projected into a unified spatial grid with an effective resolution of 1 km, providing a harmonized dataset for machine learning-based $PM_{2.5}$ modelling.

A comprehensive multi-sensor dataset was constructed to represent aerosol properties, atmospheric composition, and meteorological conditions relevant to surface $PM_{2.5}$ dynamics with retrieved from GEE dataset. Aerosol characteristics were captured using the Absorbing Aerosol Index (AAI) derived from the Sentinel-5P TROPOMI instrument (COPERNICUS/S5P/OFFL/L3_AER_AI), which provides daily observations at an approximate spatial resolution of 7×3.5 km. To further represent atmospheric chemical composition associated with biomass burning and anthropogenic emissions, trace gas columns including Nitrogen Dioxide (NO_2), Sulfur Dioxide (SO_2), Carbon Monoxide (CO), and Formaldehyde (HCHO) were obtained from corresponding Sentinel-5P TROPOMI Level-3 products. All trace gas variables were processed using a 3-day temporal window and aggregated into daily mean values to reduce noise and account for data gaps caused by cloud cover and retrieval uncertainties.

Meteorological conditions were incorporated using ERA5-Land reanalysis data (ECMWF/ERA5_LAND/HOURLY), which provides hourly variables at a spatial resolution of approximately 9 km. Key variables included 2 m air temperature (T2m), 2 m dew point temperature (D2m), 10 m wind components (U10 and V10), total precipitation (TP), and surface pressure (SP). These variables were aggregated into daily mean values to ensure temporal consistency with satellite-derived predictors. Derived meteorological parameters were also calculated, including relative humidity (RH2m), computed diagnostically from T2m and D2m following established formulations, and wind speed (WS10), derived from vector components U10 and V10. In addition, atmospheric boundary layer height (BLH), representing vertical mixing conditions, was obtained from ERA5 and aggregated as a daily mean, with an effective spatial resolution of approximately 31 km.

To characterize aerosol loading more directly, AOD at wavelengths of 0.55 μm and 0.47 μm was obtained from the MODIS MAIAC product (MODIS/061/MCD19A2_GRANULES), which provides high-resolution (1 km) daily observations. These AOD products are particularly relevant for capturing fine particulate concentrations associated with smoke and haze events. All satellite and reanalysis datasets were harmonized spatially and temporally, aggregated to a daily scale, and aligned to a common grid prior to model development, ensuring consistency across variables and enabling robust integration within the machine learning framework (Balsamo et al., 2018; Bennouna et al., 2016; Berg et al., 2012; Binte Habib et al., 2025).

2.2 Methods

The in-situ AQI is calculated using the linear interpolation formula (Zaib et al., 2022):

$$AQI = \frac{I_{high} - I_{low}}{C_{high} - C_{low}}(C_p - C_{low}) + I_{low} \quad (1)$$

where C is the observed pollutant concentration, C_{low} and C_{high} are the lower and upper concentration breakpoints, and Ilow and Ihigh are the index values corresponding to those

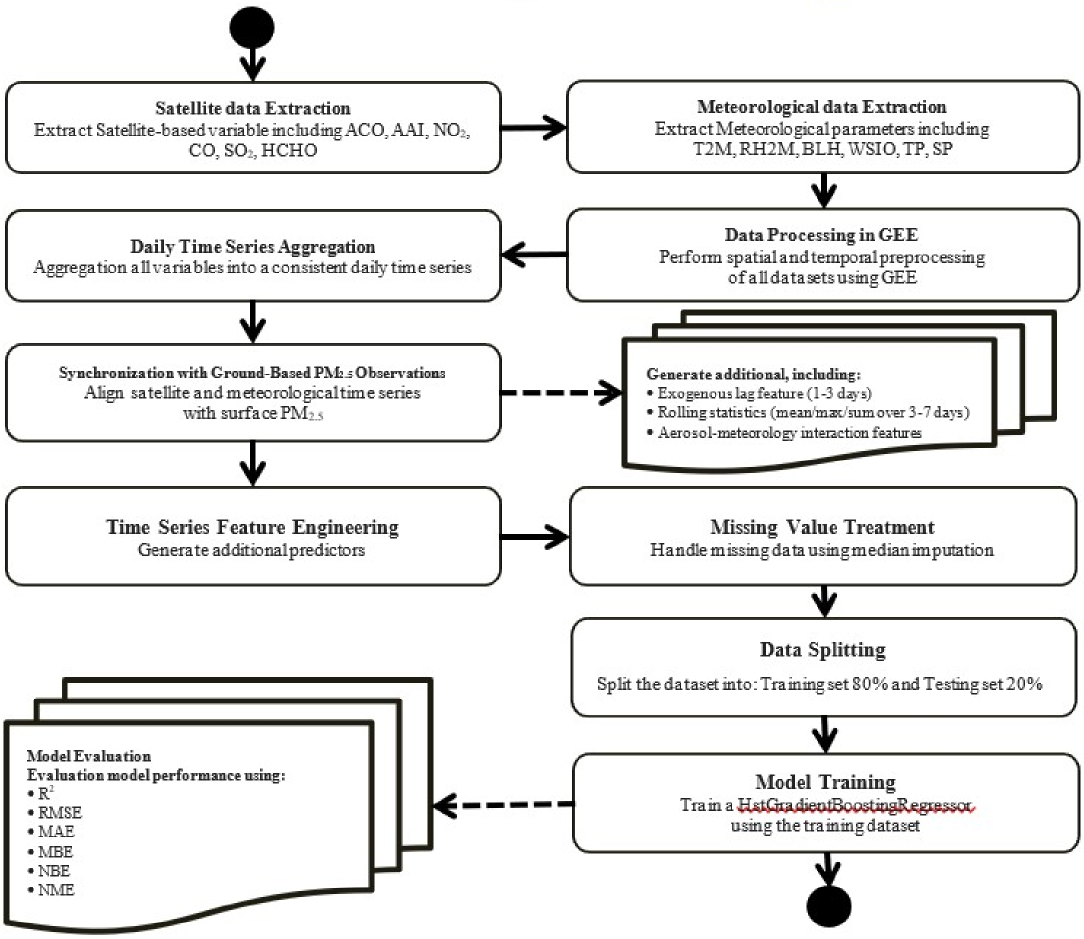

Figure 1. Integrated Workflow for Satellite Based PM$_{2.3}$ Estimation using Multi-Sensor Data, Temporal Feature Engineering, and HGBR Modeling in GEE

Table 1. Air Pollutant Standard Index Range

Category	Range
Good	0–50
Moderate	50–100
Unhealthy	100–199
Very unhealthy	200–300
Dangerous	300 and above

Source: Regulation of the Minister of Environment and Forestry No 14 of 2020, (`https://www.slideshare.net/slideshow/permen-lhk-nomor-14-tahun-2020/250526280`)

breakpoints, which for Indonesia are determined based on Table 1.

2.2.1 Satellite-Based PM$_{2.5}$ Estimation Framework

Surface PM$_{2.5}$ was estimated using a multi-sensor machine learning framework in GEE. The daily dataset integrated aerosol properties (AOD 0.55/0.47 μm, UVAI), trace gases (NO_2, CO, SO_2, HCHO), and meteorology (Temp, RH, Rainfall, Wind, PBLH) from 2021-2025. To capture atmospheric dynamics, we implemented advanced feature engineering: 1 till 3-day exogenous lags for key aerosol and weather variables, and 3 to 7-day rolling statistics (mean, max, accumulation). This approach allows the model to account for the delayed effects of smoke transport and accumulation during persistent peat fire

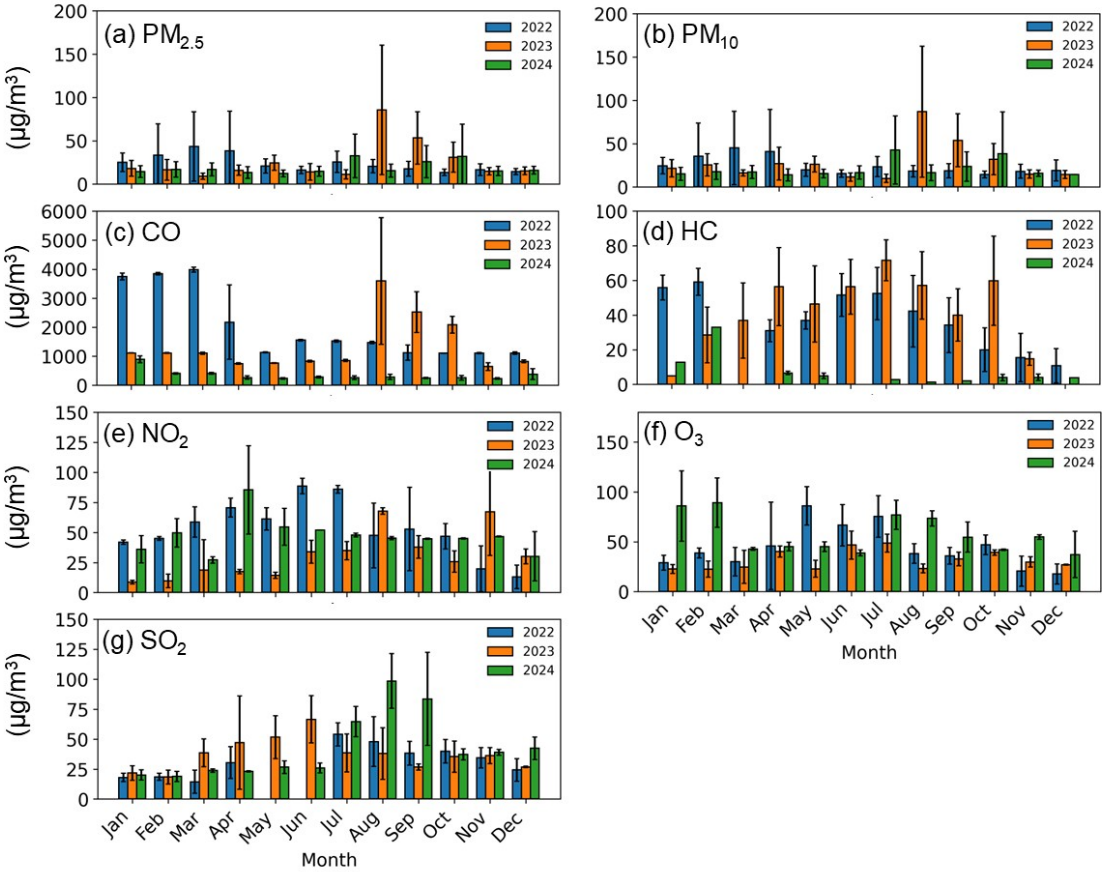

Figure 2. Monthly Average Concentrations of (a) $PM_{2.5}$, (b) PM_{10}, (c) CO, (d) HC, (e) NO_2, (f) O_3, and (g) SO_2 in Pontianak (2022–2024), where Bar Colors Denote Different Years and Error Bars Represent Standard Deviation

episodes without requiring past ground-level $PM_{2.5}$ data.

2.2.2 Temporal Feature Engineering and Data Processing

The integration of 3-day and 7-day rolling windows was implemented to represent aerosol persistence and accumulation while minimizing short-term noise in satellite observations (Guo et al., 2020). A 3-day window captures immediate variability from active fire emissions, whereas a 7-day window reflects broader weekly-scale dispersion processes (Stavros et al., 2014). Preliminary sensitivity testing indicated that extending lags beyond 3 days or using longer windows did not yield significant performance gains and increased the risk of overfitting. Thus, these selected features optimize the balance between physical atmospheric processes and model parsimony.

The data processing workflow in GEE began with the systematic acquisition of multi-sensor datasets, including Sentinel-5P, MODIS MAIAC, ERA5-Land, and fire products, covering the period from 1 January 2021 to 31 December 2025. These datasets underwent rigorous spatial and temporal filtering to align with study boundaries, followed by product-specific quality control procedures to ensure data reliability. Sub-daily and hourly observations were subsequently aggregated into daily composites and extracted using a station-based buffer approach to produce spatially representative averages for each monitoring location. Finally, these variables were integrated into a unified feature table enriched with time-series predictors, such as exogenous lags and cumulative metrics before being utilized to train and evaluate the HGBR for $PM_{2.5}$ estimation.

To better represent the physical mechanisms of particle dispersion, instantaneous interaction features were incorporated into the model. These included interactions between AOD and PBLH, AOD and Relative Humidity (RH), and UVAI and PBLH. These features allow the model to account for how vertical atmospheric structure and moisture affect surface aerosol concentrations. All predictors were consolidated into a single feature matrix, where missing values in predictor variables were handled via median imputation, while rows with missing ground-level $PM_{2.5}$ target values were excluded to maintain training integrity.

The $PM_{2.5}$ estimation was performed using the HGBR, an ensemble tree algorithm optimized for large datasets and complex non-linear interactions (Ahmed et al., 2025). The model was implemented through a structured pipeline involving imputation and regression stages, utilizing an 80/20 random split for training and validation. Hyperparameters including tree

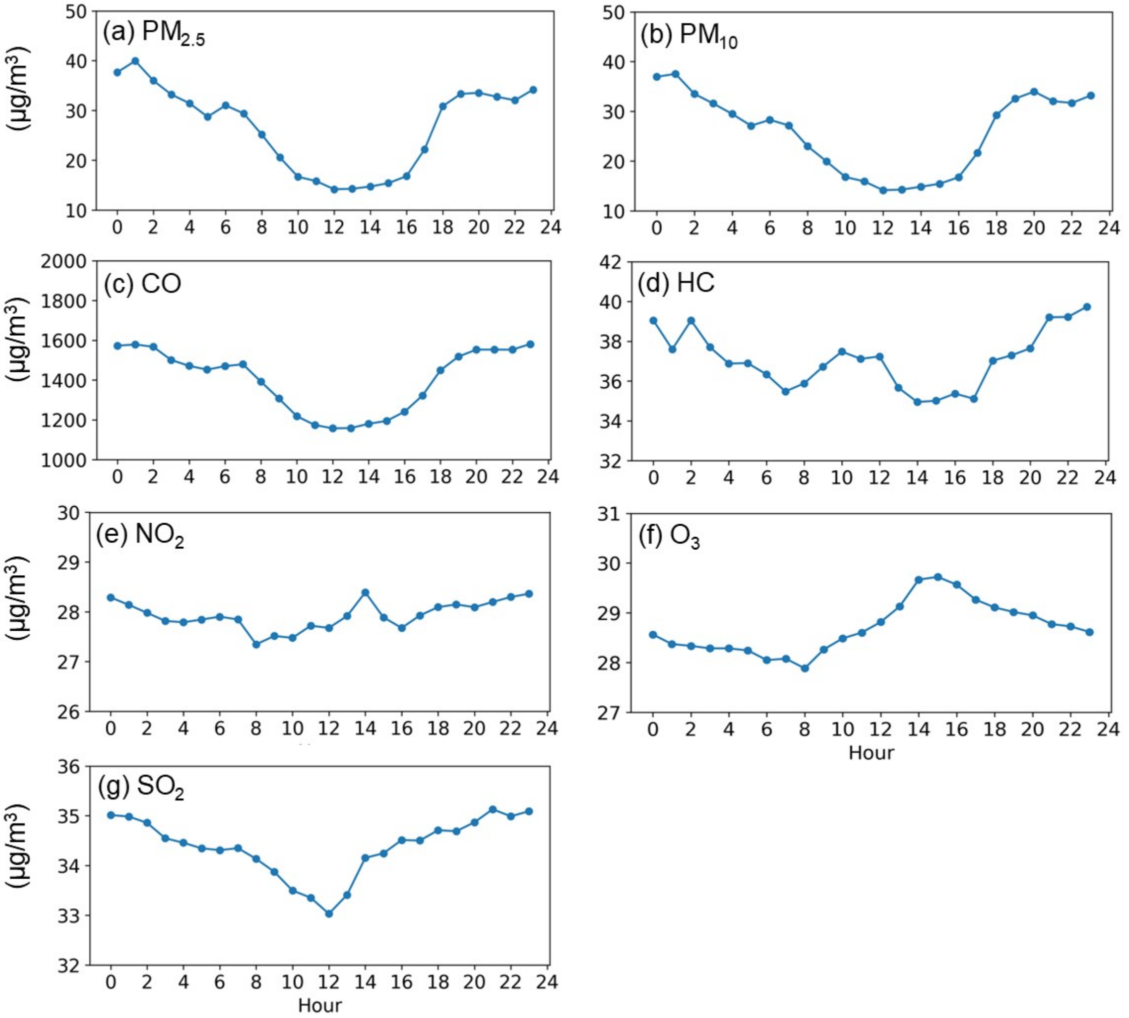

Figure 3. Diurnal Variations of (a) $PM_{2.5}$, (b) PM_{10}, (c) CO, (d) HC, (e) NO_2, (f) O_3, and (g) SO_2 in Pontianak 2023, Reflecting the Interplay Between Traffic Cycles and Planetary Boundary Layer Dynamics

depth, learning rate, and regularization were refined through a prior tuning process to ensure optimal performance. Mathematically, the $PM_{2.5}$ concentration is modeled as an additive sum of regression trees (Guryanov, 2019):

$$Y_i = \sum_{m=1}^{M} \nu \, h_m(x_i) \tag{2}$$

where Y_i is the surface $PM_{2.5}$ estimate, x_i is the vector of satellite and meteorology-based predictor features, $h_m(x_i)$ is the decision tree function for the, M is the number of iterations, and ν is the learning rate. This HGBR model implicitly minimizes the squared error and utilizes a histogram-based approach to enhance computational efficiency and estimation stability.

Model performance was evaluated using the coefficient of determination (R^2), Root Mean Square Error (RMSE), and Mean Absolute Error (MAE) (Doreswamy et al., 2020). To capture systematic tendencies, model bias was assessed through Mean Bias Error (MBE), Normalized Mean Bias (NMB), and Normalized Mean Error (NME) (Gustafson and Yu, 2012). While MBE provides the absolute average deviation, NMB and NME offer standardized metrics for comparing model performance across varying concentration ranges and pollution levels during the 2021-2025 fire periods.

2.2.3 Model Benchmarking and Independent Validation

To evaluate the robustness of the proposed framework, the HGBR was compared against several benchmark algorithms: Multiple Linear Regression (MLR) as a baseline (Uyanık and Güler, 2013), Random Forest (RF) (Breiman, 2001; Shofiana et al., 2025), and Extreme Gradient Boosting (XGBoost) (Subhi Malallah and Bahjat Abdulrazzaq, 2023). All models utilized the same predictor variables, preprocessing pipeline, and an identical 80:20 train test split to ensure objective per-

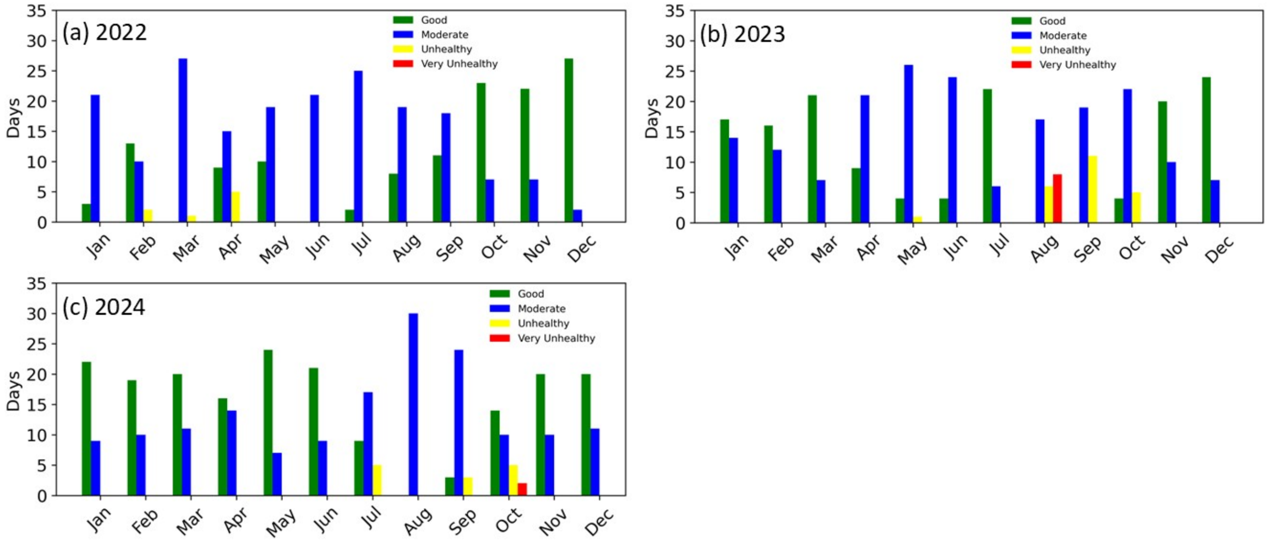

Figure 4. Monthly AQI Distribution in Pontianak for (a) 2022, (b) 2023, and (c) 2024, Illustrating Inter Annual Variability and the Bimodal Pollution Cycle

formance assessment in capturing nonlinear relationships.

Furthermore, independent validation was conducted by comparing HGBR derived weekly $PM_{2.5}$ estimates integrated with 3-day and 7-day temporal features against independent observations from the BMKG Supadio Station. This comparison focused on the year 2023, with a particular emphasis on the peak fire period to assess model performance under extreme pollution events driven by biomass burning. This step ensures the model's reliability beyond the primary training dataset. The following flowchart illustrates the complete methodology for satellite-based $PM_{2.5}$ estimation, including the comprehensive evaluation metrics (R^2, RMSE, MAE, MBE, NMB, and NME) used to verify the model's accuracy and bias. The following flowchart illustrates the complete methodology for satellite-based $PM_{2.5}$ estimation (Figure 1).

2.2.4 Hotspot Detection and Burned Area Validation

A hotspot is identified as a pixel with a significantly higher surface temperature relative to its surroundings, detected via thermal radiation in mid-wave infrared channels. In the context of forest and land fires, these thermal anomalies serve as primary indicators of active burning. However, hotspots may also originate from non-fire sources such as mining activities, industrial factories, or urban heat islands. To ensure the accuracy of fire related hotspots in this study, detections were cross referenced with temporal satellite imagery to confirm active fire events on specific dates. Furthermore, spatial data on the actual extent of forest and land fires were obtained from the official burned area records of the Ministry of Environment and Forestry (KLHK) (Vetrita et al., 2025a).

3. RESULTS AND DISCUSSIONS

3.1 Temporal Variability of Air Quality Parameters

The analysis of multi-pollutant concentrations, including CO, $PM_{2.5}$, PM_{10}, NO_2, SO_2, O_3, and HC in Pontianak, reveals distinct inter-annual and seasonal contrasts. The year 2023 emerged as the most polluted period, characterized by a significant surge in CO, $PM_{2.5}$, PM_{10}, and HC concentrations compared to 2022 and 2024, as illustrated in Figure 2. The most critical degradation in air quality occurred during the dry season, specifically from July to September. During the peak fire episodes of 2023, monthly averages reached alarming levels, with $PM_{2.5}$ peaking at approximately 100 $\mu g/m^3$, CO at 4000 $\mu g/m^3$, and both HC and NO_2 remaining consistently around 70 $\mu g/m^3$.

Conversely, O_3 concentrations exhibited a significant decline during intense forest fire events. This phenomenon is likely driven by chemical scavenging mechanisms, where high concentrations of NO_x and VOCs emitted from biomass burning react with and deplete existing ozone. Furthermore, high particulate matter loading not only directly absorbs O_3 but also attenuates UV radiation through smoke shading effects, which subsequently inhibits the photochemical reactions necessary for surface ozone formation.

While 2023 was dominated by large-scale fires, the air quality profile of 2022, a La Niña year characterized by high rainfall (Figure 2), highlights the persistent impact of urban mobile sources. In downtown Pontianak, consistently elevated CO and HC levels during non-haze periods, such as January to March 2022, serve as strong indicators of incomplete combustion from motor vehicles. The high traffic density in the provincial capital leads to frequent idling and low RPM engine operation, which significantly increases CO production, particularly in poorly maintained vehicles with low combustion efficiency (Aziis et al., 2025; Yulianti et al., 2024). These findings validate that vehicle emissions remain the primary pollutant source in Pontianak in the absence of land fires, although during the March May (MAM) transition season, even minor rainfall reductions can trigger $PM_{2.5}$ spikes reaching levels unhealthy for sensitive groups.

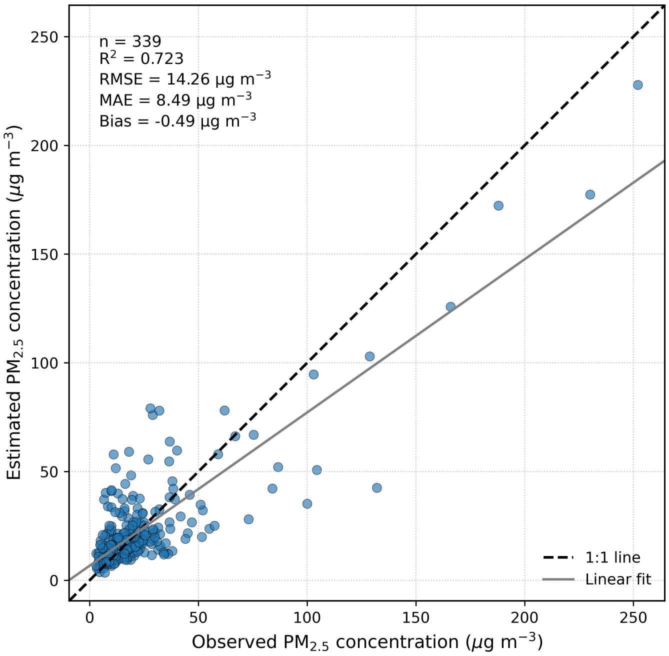

Figure 5. Scatter Plot of Observed Versus Satellite Estimated $PM_{2.5}$ Concentrations for the Test Dataset. Observed vs Predicted (R^2=0.723, RMSE=14.26, MAE=8.49)

3.1.1 Diurnal Variations and Atmospheric Drivers

The diurnal profiles of pollutants in Pontianak exhibit a strong coupling between anthropogenic activities and Planetary Boundary Layer Height (PBLH) dynamics (Figure 3). Concentrations of $PM_{2.5}$ and PM_{10} typically rise between 09:00 and 21:00 UTC (16:00–04:00 WIB), coinciding with evening rush hours and nocturnal PBLH compression. During the night, the significant decrease in PBLH traps particulates near the surface, leading to peak concentrations (The Impact of Atmospheric Stability Affected by Peat Forest Fire on Surface $PM_{2.5}$ Concentration in Pontianak Urban Area during La Nina Events 2022, 2024).

Similarly, traffic-related pollutants such as CO, NO_2, and HC peak during morning and evening commuting hours, reflecting the dominant contribution of motor vehicle emissions in Pontianak's urban core. These levels dissipate at midnight and mid-day when traffic volume decreases and atmospheric dispersion improves. Conversely, O_3 follows an opposite trend, peaking during daylight hours (05:00 - 09:00 UTC) due to intense photochemical production, further confirming the influence of solar radiation and precursor availability on diurnal air quality fluctuations.

The diurnal profile of O_3 as a secondary pollutant is characterized by a midday-to-evening peak, driven by photochemical reactions of precursors (NO_x and HC) under intense solar radiation (Figure 3). Conversely, nocturnal O_3 levels remain negligible. For SO_2, distribution patterns in Pontianak are primarily influenced by localized industrial and transportation cycles, though meteorological conditions remain the overarching driver for all pollutants.

Meteorological parameters exert a significant control over air quality; rainfall shows a strong negative correlation with $PM_{2.5}$ through atmospheric scavenging, while air temperature and low wind speeds facilitate pollutant accumulation. Notably, the 2023 El Niño event exacerbated these conditions by extending the dry season and reducing precipitation, which increased the frequency of peatland fires (Aziis et al., 2025). These anomalies drastically elevated $PM_{2.5}$ and PM_{10} concentrations far beyond safety thresholds, effectively overriding normal diurnal patterns with extreme pollution spikes. This highlights Pontianak's high vulnerability to smoke disasters during climatically driven fire seasons.

3.1.2 AQI Evaluation and the Bimodal Pollution Cycle

The AQI in Pontianak reveals a distinctive bimodal cycle driven by the region's equatorial climate (Figure 4). In 2022, Moderate conditions dominated (58.4%), yet Unhealthy spikes (2.4%) during February - April confirmed a secondary peak during the first dry season. This phase is characterized by reduced rainfall and dry surface winds that transport smoke from surrounding peatlands into the city.

Air quality significantly deteriorated in 2023, with "Unhealthy" and "Very Unhealthy" days rising to 6.4% and 2.2%, respectively. This degradation, particularly the "Very Unhealthy" episodes in August, aligns with increased hotspot counts and surface temperature anomalies intensified by the 2023 El Niño event (Aziis et al., 2025). Conversely, 2024 showed marked improvement, with Good days rising to 51.5% as fire frequency decreased. These fluctuations validate that Pontianak's air quality is sensitive to both the bimodal dry season cycle and larger climatic drivers.

3.2 Model Performance and Comparative Validation

The HGBR model demonstrates robust predictive capability for surface $PM_{2.5}$ estimation, achieving a coefficient of determination (R^2) of 0.723, with RMSE and MAE values of 14.26 $\mu g/m^3$ and 8.49 $\mu g/m^3$, respectively (Table 3 and Figure 5). This performance indicates that the integrated satellite-meteorological feature space explains over 70% of the daily $PM_{2.5}$ variability in Pontianak. The model's success is attributed to its optimized configuration including L_2 regularization (10.0) and a learning rate of 0.03, which effectively captures non-linear relationships between multi-sensor predictors and surface concentrations while preventing overfitting.

Table 2. Comparative Performance of Machine Learning Models for $PM_{2.5}$ Estimation

Model	R^2	RMSE	MAE	MBE	NMB	NME	n
HGBR	0.723419	14.25789	8.487559	0.488512	0.023147	0.40217	339
XGB	0.688091	15.14114	8.640199	0.3384	0.016035	0.409403	339
RF	0.67312	15.50023	8.902693	0.652266	0.030907	0.421841	339
MLR	0.509385	18.98955	11.94902	0.826386	0.039157	0.566187	339

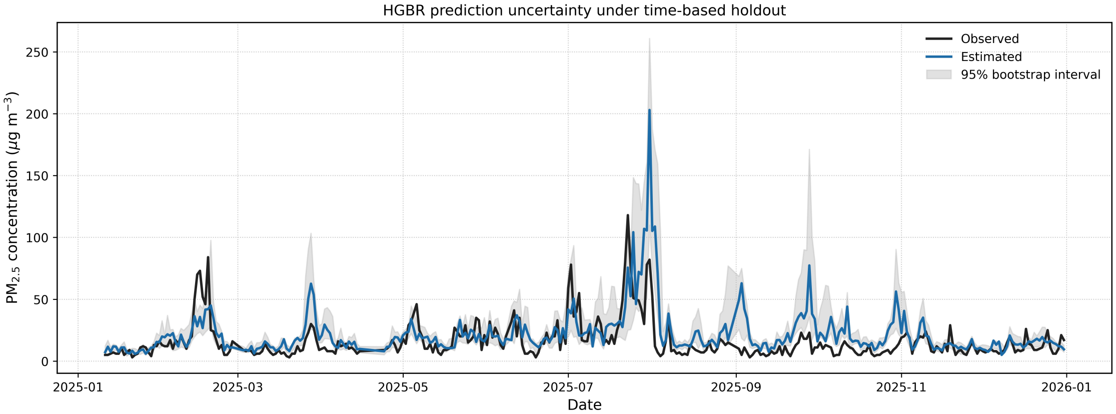

Figure 6. Time Series of Observed Versus HGBR Estimated Daily $PM_{2.5}$ Concentrations from 2021 to 2025, Including a 95% Bootstrap Confidence Interval to Illustrate Model Stability Across Different Pollution Regimes

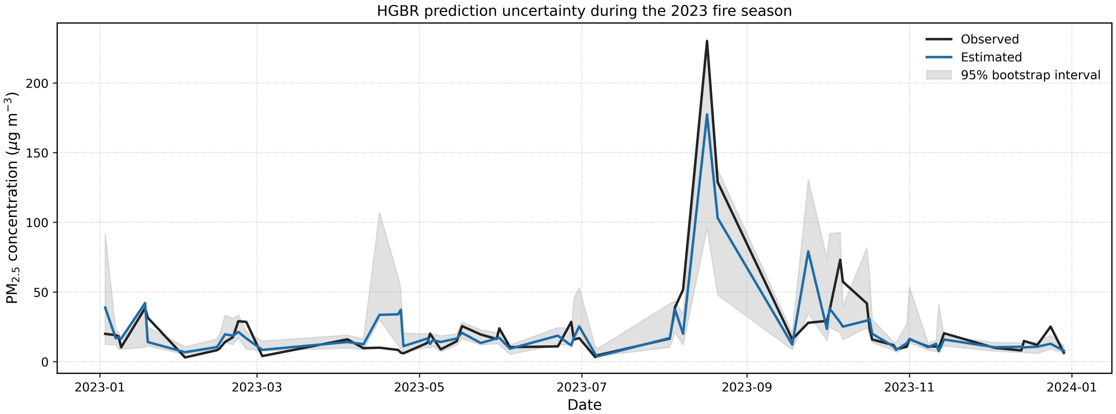

Figure 7. Temporal Validation of HGBR Estimated $PM_{2.5}$ of the 2023 Fire Season Highlighting The Model's Capability to Capture Extreme Pollution Surges Within a 95% Bootstrap Confidence Interval

Table 3. Sensitivity Analysis of Temporal Rolling Window Features (3-Day, 7-Day, and Combined) and Their Impact on Model Performance Metrics

R^2	RMSE	MAE	MBE	NMB	NME	n	configuration
0.670808	15.55495	9.118838	0.508508	0.024095	0.432083	339	3-day
0.682098	15.2859	9.214483	0.194259	0.009205	0.436615	339	7-day
0.723419	14.25789	8.487559	0.488512	0.023147	0.40217	339	combined

Comparative analysis reveals that the HGBR approach significantly outperforms other machine learning benchmarks and traditional linear methods (Table 2). While XGBoost and Random Forest achieved competitive R^2 values (0.688 and 0.673), they exhibited higher error metrics compared to HGBR. In contrast, Multiple Linear Regression (MLR) showed substantially weaker performance (R^2 = 0.509), highlighting its inability to model complex atmospheric interactions. Bias metrics

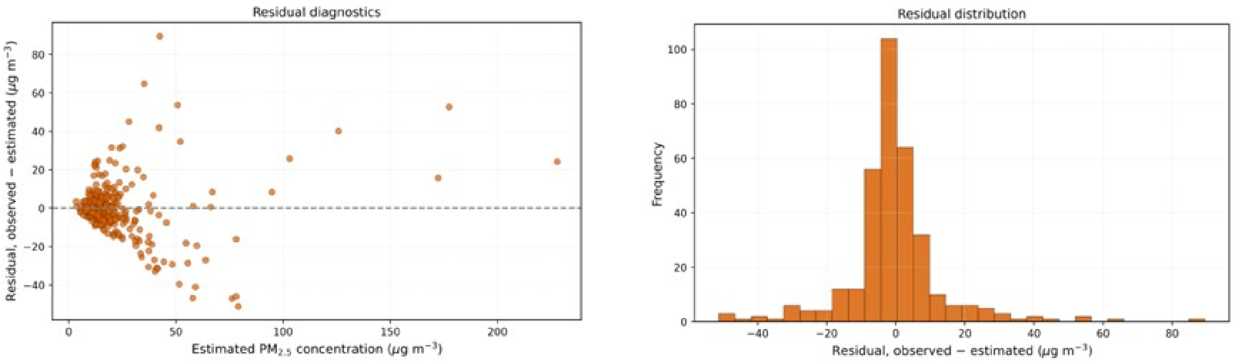

(a) (b)

Figure 8. Residual Diagnostics of the HGBR Model Showing: (a) Predicted $PM_{2.5}$ versus Residuals, and (b) Frequency Distribution of the Estimation Residuals

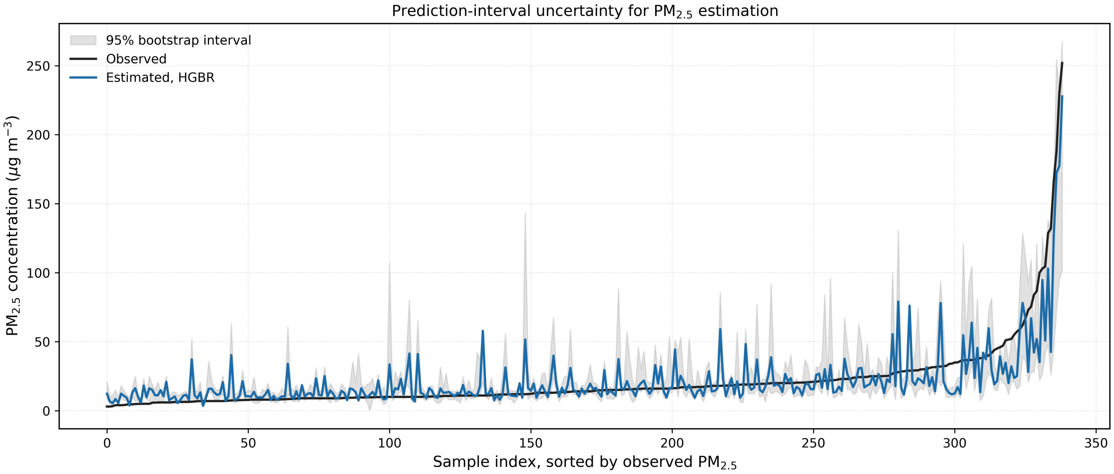

Figure 9. Prediction Interval Based Uncertainty Analysis of $PM_{2.5}$ Estimation, Illustrating the 95% Prediction Interval and Model Robustness Across the Observed Concentration Range

(MBE, NMB, NME) further confirm that HGBR provides the most balanced error distribution, despite a slight tendency to underestimate extreme concentrations a common challenge in satellite-based estimation due to aerosol optical saturation (Bennouna et al., 2016). The superiority of HGBR stems from its histogram-based tree construction, which enhances computational stability when handling heterogeneous datasets with high multicollinearity.

3.2.1 Temporal Performance of Satellite-Based $PM_{2.5}$ Estimation

The HGBR estimated and observed $PM_{2.5}$ time series (2021-2025) demonstrate high temporal consistency, accurately tracking daily fluctuations and extreme episodic spikes (Figure 6). Across the multi-year period, the model effectively reproduces dominant seasonal patterns, identifying low-concentration background levels during wet seasons and sharp pollution surges during dry seasons. This alignment confirms that the integration of multi-sensor predictors and temporal features successfully captures persistent atmospheric dynamics rather than random daily variations.

The model's robustness is most evident during the extreme 2023 fire season. While pre-fire estimates (January-June) closely follow urban background conditions, the model captures the rapid onset of the August-September surge, with estimated values exceeding 150 $\mu g/m^3$ in sync with observations. Despite a slight dampening of peak amplitudes likely due to satellite signal saturation under dense aerosol loading, the temporal duration and post-fire decay phase are well-represented. This capability indicates that the model effectively represents the temporal memory characteristic of peat-burning aerosols (Huang and Rein, 2014).

Furthermore, the 95% bootstrap Confidence Interval (CI) in Figure 7 confirms the stability of the HGBR framework during consecutive haze days. While deviations on high AOD days reflect inherent limitations in vertical aerosol representa-

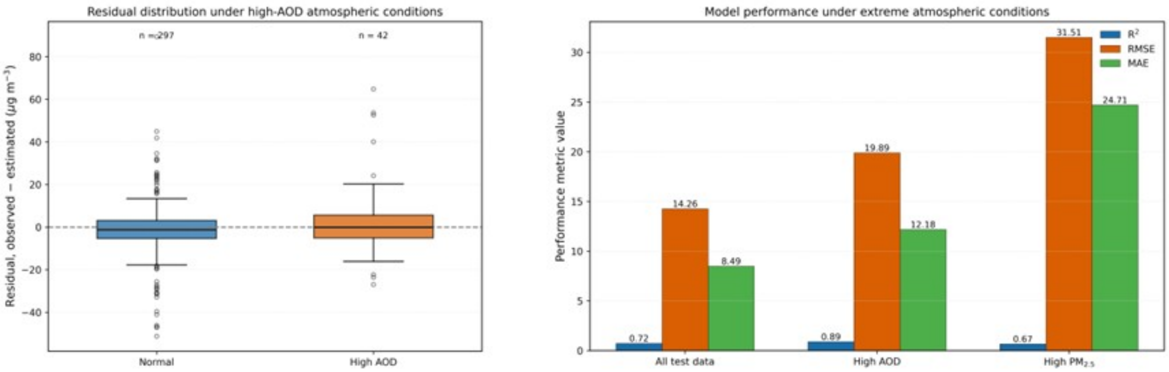

(a) (b)

Figure 10. (a) Residual Distribution of $PM_{2.5}$ Estimation under Normal and High AOD Conditions and (b) Model Performance under Extreme Conditions with Emphasis on R^2, RMSE, and MAE

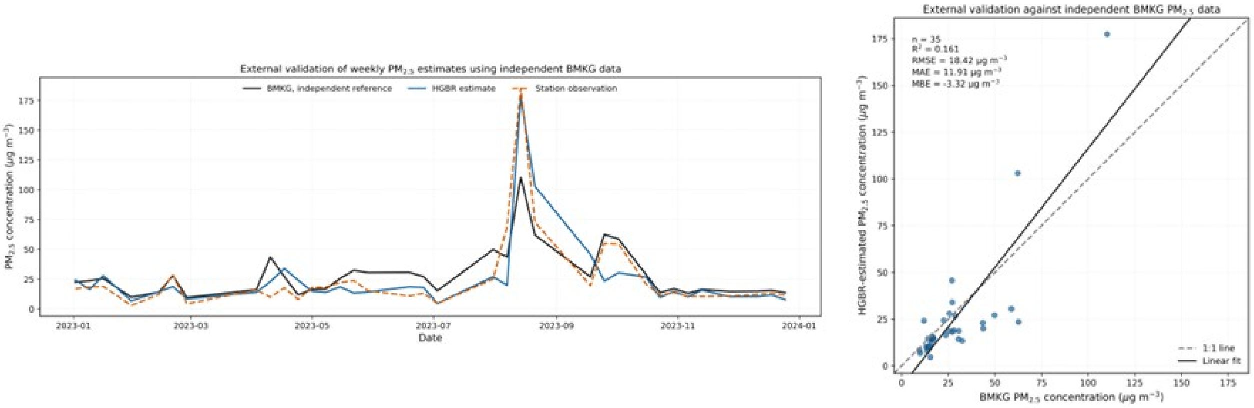

(a) (b)

Figure 11. External Validation for 2023: (a) Scatter Plot of Weekly $PM_{2.5}$ from HGBR versus BMKG Observations at Supadio, and (b) Weekly Time Series Comparison of $PM_{2.5}$ from BMKG, Station Observations, and HGBR Estimates

tion, the overall results validate this approach for long-term air quality monitoring and early warning systems in smoke-prone regions like Pontianak. The temporal performance of the HGBR model in this study outperforms previous satellite-based $PM_{2.5}$ models, which often struggle to reproduce daily spikes and smoke persistence during intense fire episodes (Ravish et al., 2025). While earlier studies relying on single AOD or linear regression approaches typically captured only broad seasonal trends, they frequently failed to represent the duration of multi-day haze events and post-fire decay phases (Kong et al., 2016).

3.2.2 Error Characteristics and Bias Behaviour

Residual analysis indicates that model errors are non-randomly distributed and are dependent on $PM_{2.5}$ concentration levels. At low-to-medium ranges, residuals are densely centered around zero, suggesting no systematic bias under background urban conditions. This stability confirms the model's proficiency in representing daily $PM_{2.5}$ variations driven by normal meteorological cycles. Conversely, at high concentrations during intense fire episodes, residuals exhibit increased variance and a negative bias (underestimation). This heteroscedastic pattern implies that model uncertainty escalates with atmospheric aerosol load, a common challenge in satellite-based estimation due to vertical aerosol mismatch and limited signal sensitivity at extreme values (Atkinson et al., 2016; Karim et al., 2025). The overall residual distribution remains centered at zero but features a long right tail, reflecting extreme events where in-situ observations exceed model estimates.

The observed error patterns align with existing literature on satellite-based $PM_{2.5}$ estimation in biomass-burning regions. While previous studies often report significant heteroscedas-

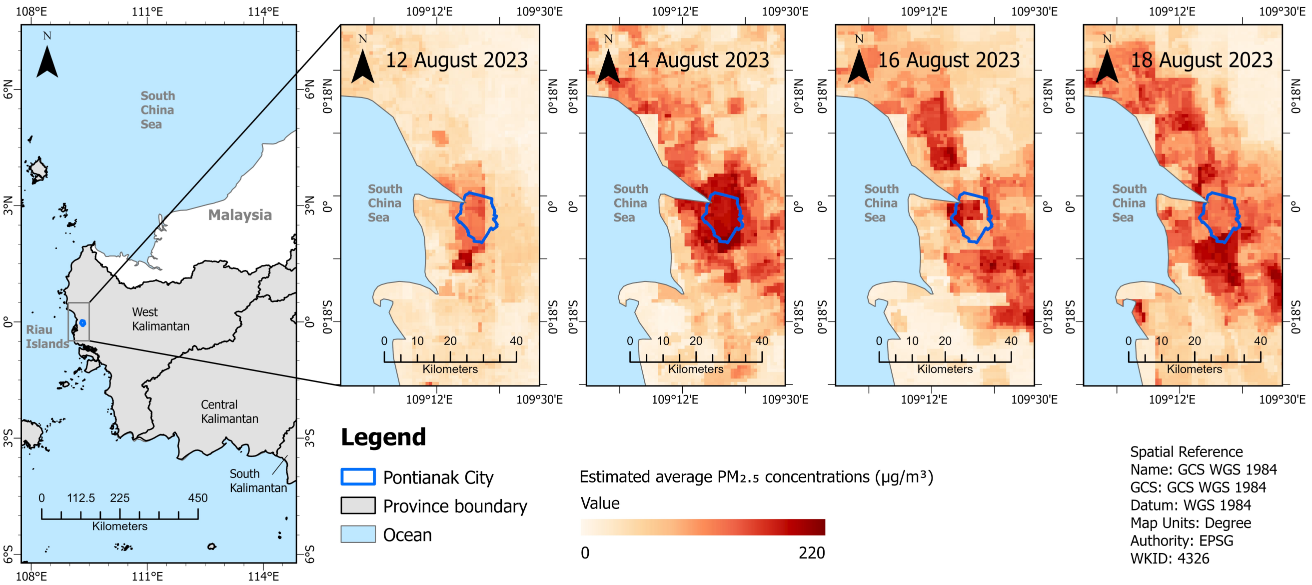

Figure 12. Spatial Distribution of Estimated Daily Average $PM_{2.5}$ Concentrations Across Pontianak and Surrounding Areas for Selected Dates between August 12 and 18, 2023

ticity and negative bias during intense haze attributed to AOD signal saturation and vertical aerosol mismatch (Handschuh et al., 2024; Karim et al., 2025), the HGBR model in Pontianak achieves a more stable and centered residual distribution (Figure 8).

3.2.3 Uncertainty Analysis and Model Robustness

Uncertainty propagation was examined through sensitivity analysis of temporal feature configurations (Table 3 and Figure 9). Results demonstrate that integrating both short-term (3-day) and medium-term (7-day) rolling windows significantly enhances predictive accuracy, achieving the highest R^2 (0.723) and lowest RMSE (14.26 $\mu g/m^3$) compared to single-window configurations. This combined approach effectively captures the short-term persistence of smoldering peat fires and weekly-scale smoothing effects, minimizing prediction variance during dynamic atmospheric changes.

The selection of 1-3 days lags and 3-7 days rolling statistics is supported by the physical characteristics of tropical peat fire environments, where limited dispersion often results in multi-day pollution episodes. Sensitivity experiments show that models excluding these temporal features suffer from increased residual dispersion and reduced generalization, particularly during peak events. By explicitly modelling these dependencies, the HGBR framework balances atmospheric memory with model parsimony, ensuring both temporal stability and robust performance under varying emission regimes (Binte Habib et al., 2025).

3.2.4 Performance under High-AOD and Extreme Conditions

The HGBR model exhibits regime-dependent error characteristics, with increased uncertainty during high-AOD and extreme $PM_{2.5}$ episodes (Figure 10). Residual analysis shows that under normal conditions, errors are tightly centered around zero with minimal bias. In contrast, high-AOD scenarios exhibit broader residual spreads and a tendency toward underestimation, reflecting the inherent limitations of satellite proxies under dense haze (Chen et al., 2016). Comparative performance metrics reveal that while the model maintains high sensitivity to aerosol variability, achieving its highest explanatory power (R^2 = 0.89) during high-AOD events, absolute error increases significantly during extreme $PM_{2.5}$ episodes (RMSE = 31.5 $\mu g/m^3$). This degradation underscores the challenge of capturing nonlinear pollution peaks compared to the balanced performance observed across the full dataset (R^2 = 0.72, RMSE = 14.3 $\mu g/m^3$). These results confirm that while HGBR is robust for general monitoring, predictive uncertainty escalates during severe haze events, necessitating caution in interpreting peak concentrations.

3.2.5 Uncertainty Sources and External Validation

While the HGBR model demonstrates high accuracy, certain uncertainties remain inherent in satellite-based $PM_{2.5}$ estimation. Column-integrated properties (AOD/AAI) may not fully capture near-surface stratification, especially during signal saturation in extreme fire events. Additionally, spatial resampling and temporal lag-based engineering introduce minor representativeness errors during severe haze episodes (Figure 11a).

External validation against independent Indonesian Agency

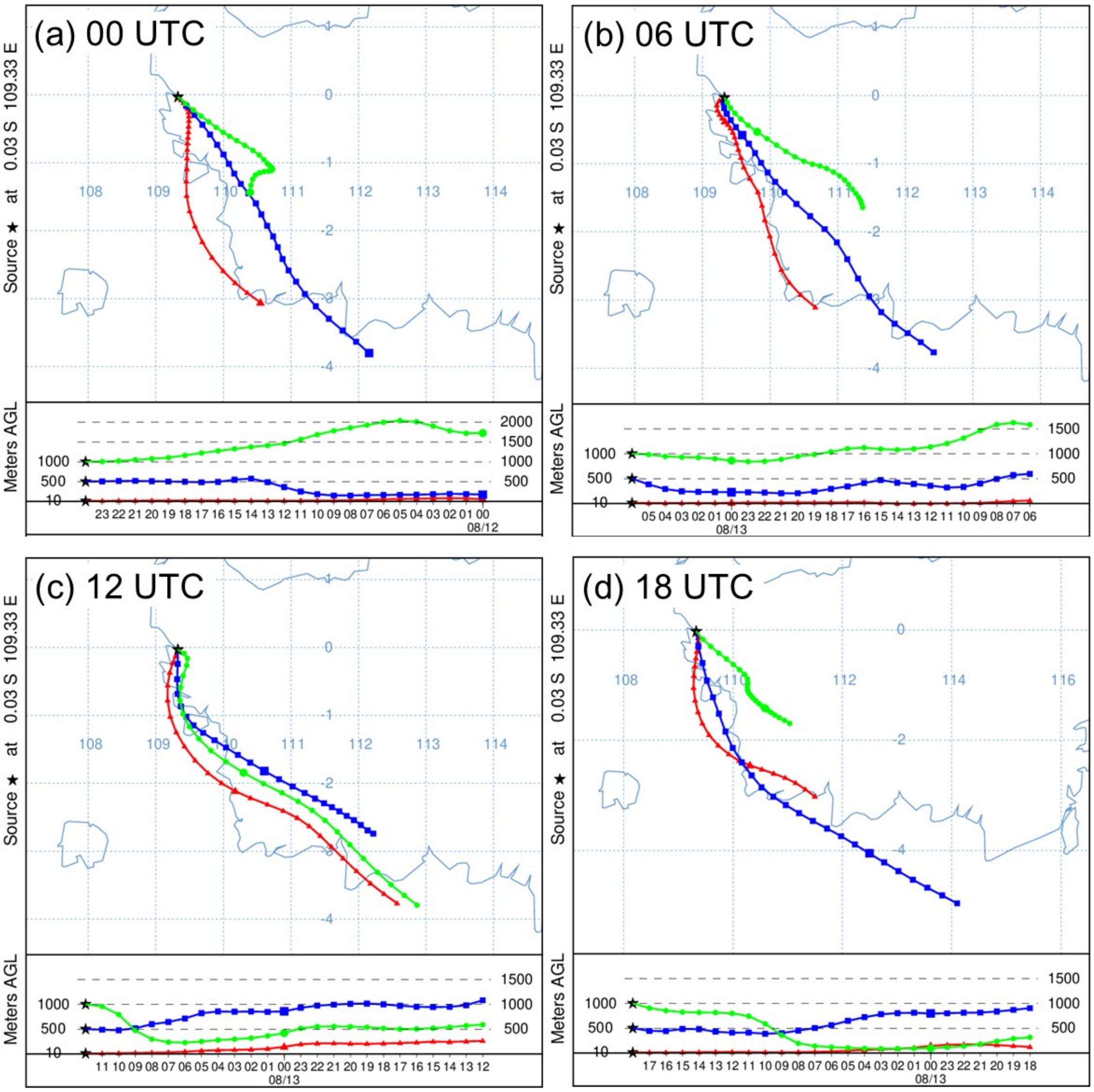

Figure 13. 24-Hour HYSPLIT Backward Trajectories Ending at Pontianak on 13 August 2023 at Altitudes of 10 m (Red), 500 m (Blue), and 1000 m (Green) Above Ground Level. Panels Show Trajectories Ending at (a) 00:00 UTC, (b) 06:00 UTC, (c) 12:00 UTC, and (d) 18:00 UTC

for Meteorological, Climatological and Geophysics (BMKG) data (Figure 11b) confirms the model's reliability in tracking the 2023 biomass burning season. Although the scatter analysis (Figure 11b, right panel) yields a lower R^2 (0.16), this reflects structural differences: BMKG data are weekly averages which smooth daily variability and compress peak values. During the August–September peak, BMKG reported ~110 μg/m^3, while HGBR estimates correctly identified surges exceeding 170 μg/m^3 in sync with station observations. This suggests that the HGBR framework maintains superior sensitivity to surface pollution dynamics compared to weekly-aggregated external protocols (Coelho et al., 2008).

3.2.6 Spatial Patterns of $PM_{2.5}$ Estimates

Daily $PM_{2.5}$ maps for August 9 - 28, 2023, effectively capture the spatiotemporal evolution of a major haze episode (Figure 12). During the early phase (Aug 9 - 11), concentrations were low and localized. By mid-August, rapid expansion occurred with high-concentration clusters forming over Pontianak and coastal areas, driven by polluted air masses from southeastern fire sources (Yin et al., 2019).

The event peaked between August 14 and 18, showing widespread, high-intensity $PM_{2.5}$ concentrations across the study area. This uniform distribution reflects regional aerosol transport from intense peat fires. Subsequently, the plume fragmented and returned to near-background levels by August 26-28 as fire activity subsided. The model's ability to

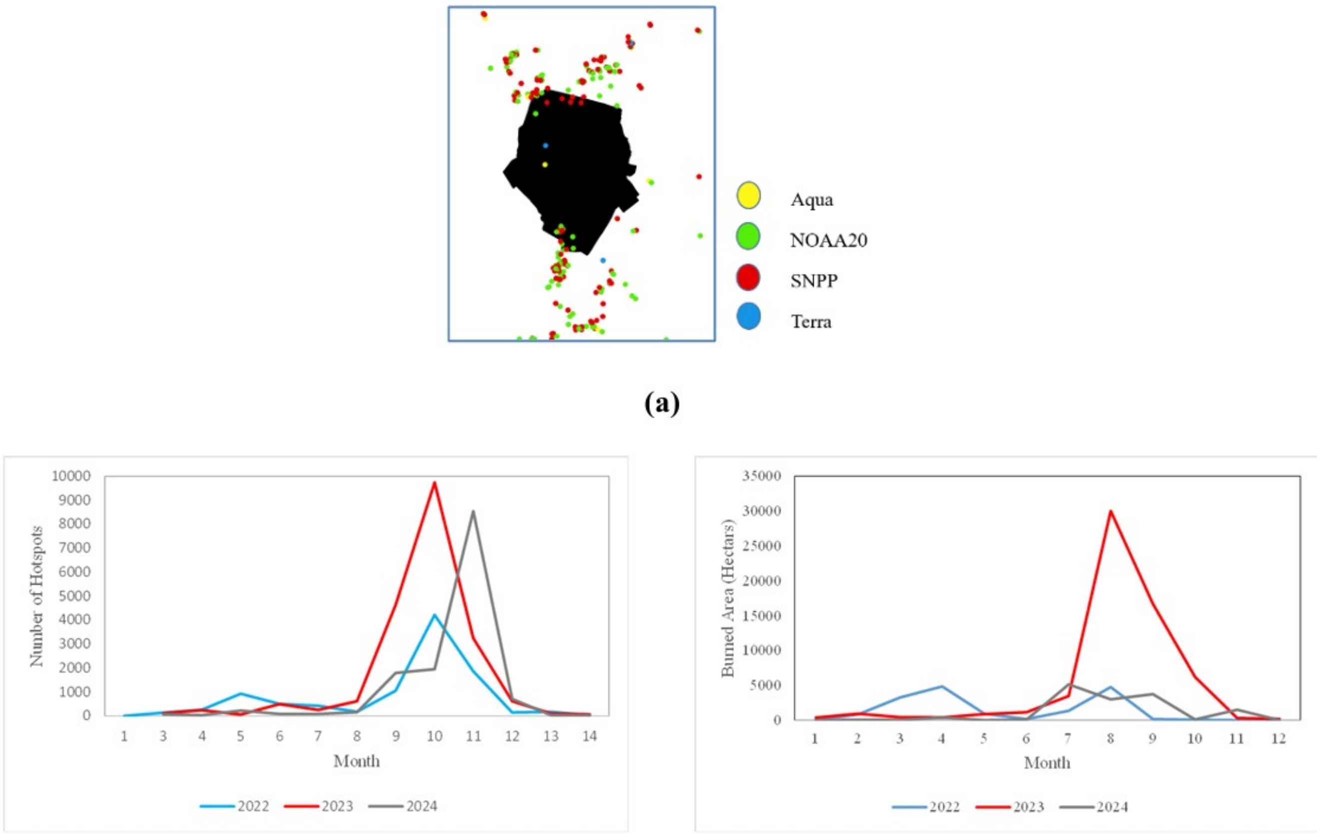

(a)

(b)   (c)

Figure 14. Forest and Land Fire Indicators for the 2022-2024 Study Period: (a) Spatial Distribution of Hotspots from NOAA-20, SNPP, and MODIS Satellites, and (Bottom) Monthly Distribution of Total Hotspot Counts (b) and Burned Area (c) in Hectares

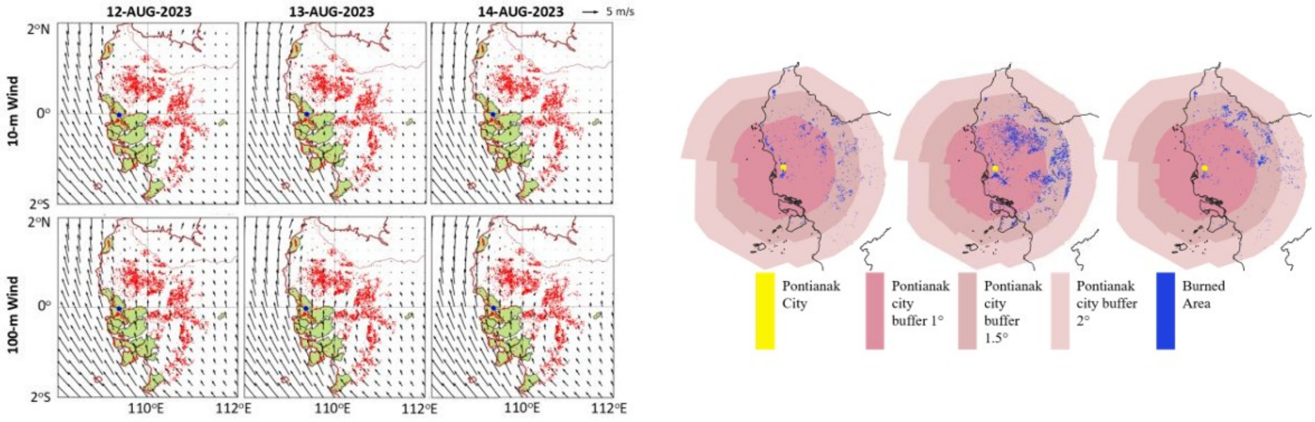

(a)   (b)

Figure 15. Spatial Drivers of the 2023 Haze Episode: (a) ERA5 Daily Average Wind Field (Speed and Direction) at 10 m and 100 m Levels Overlaid with Active Fire Locations (12-14 August 2023); and (b) Spatial Distribution of BA Around Pontianak City using Incremental Buffers up to 2° for the Years 2022, 2023, and 2024. The Blue Clusters Highlight the Extensive BA Occurring in August 2023

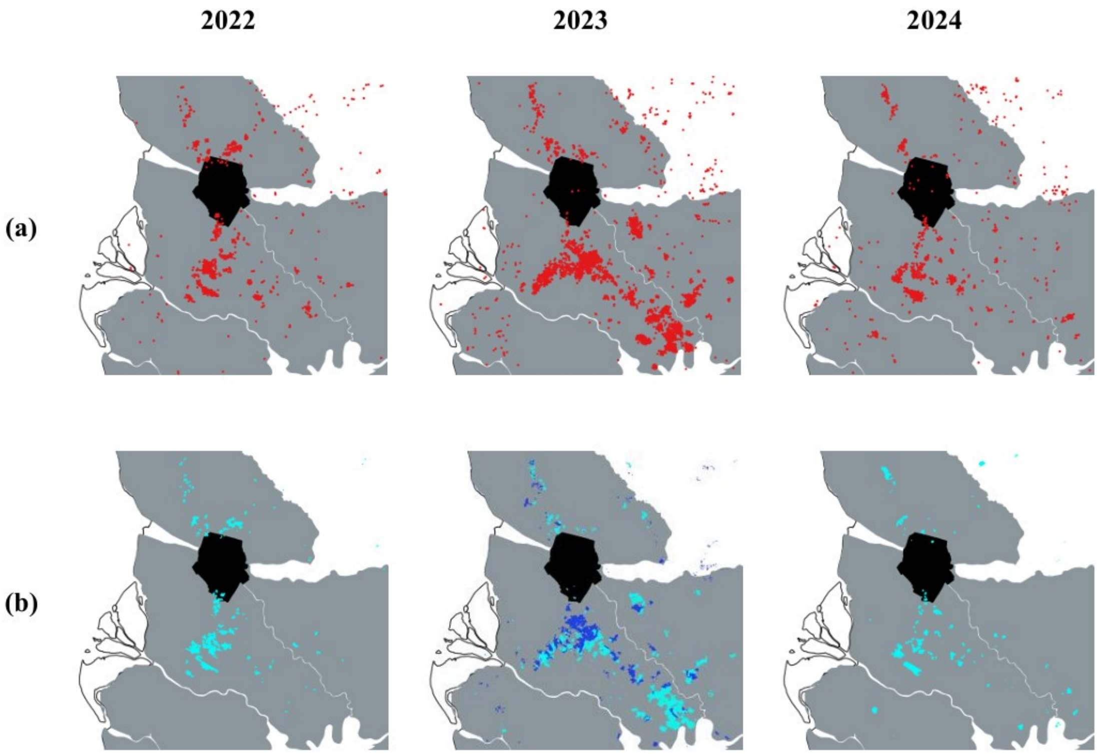

Figure 16. Distribution of Hotspots (a) and BA (b) in 2022, 2023, and 2024, Respectively. Clustered Hotspots are Closely Related to the Presence of BA. In 2023, the Dark Blue Burn Area Indicates BA that Occurred in August

realistically represent the expansion and contraction of $PM_{2.5}$ exposure areas reinforces its value for population exposure analysis and operational air quality monitoring.

The observed spatial patterns align with previous research on Southeast Asian biomass fires, which typically report regional $PM_{2.5}$ expansion during peak fire phases followed by gradual dispersion (Ma et al., 2022). While earlier studies using single-AOD or static approaches often only captured seasonal averages, the HGBR model in Pontianak successfully represents daily transitions from onset to recovery. Compared to more fragmented spatial patterns reported in previous studies (Xu et al., 2020), this multi-sensor approach provides a more stable and realistic representation of aerosol transport and peat-burning dynamics. These results confirm that integrating aerosol, fire, and meteorological data significantly improves $PM_{2.5}$ exposure interpretation at the urban scale in smoke-prone tropical regions.

3.2.7 Pollutant Trajectory Analysis

To identify the origin of air masses during the peak pollution event, 24-hour backward trajectories were simulated using the NOAA HYSPLIT model for 13 August 2023 (Figure 13). Analysis across four time intervals (00:00 to 18:00 UTC) reveals a consistent influx of air packets from the south and southeast, aligning with the dominant East Monsoon flow from Australia. At low altitudes (10-500 m; red and blue lines), air masses primarily originated from the Java Sea and moved across the coastal peatlands of Kubu Raya before reaching Pontianak. As the most extensive peat ecosystem in West Kalimantan, fires in this region contribute dense surface smoke rich in $PM_{2.5}$ and carbon monoxide. Simultaneously, medium-to-high altitude trajectories (1000 m; green lines) show a broader regional influence, including transport from degraded peatlands in Central Kalimantan. These results confirm that the extreme $PM_{2.5}$ levels observed in Pontianak were driven by the convergence of localized emissions and regional transboundary haze from intensive peat burning areas to the southeast.

3.3 Forest and Land Fire Dynamics

The hotspots identified in this study were derived from multiple satellite sensors, including NOAA-20, SNPP, and MODIS (Aqua/Terra), ensuring comprehensive coverage of surface thermal anomalies (Figure 16). While hotspots serve as early indicators of fire activity, the actual Burned Area (BA) was quantified using established indices such as NBR and dNBR (Vetrita et al., 2025b).

The monthly distributions for 2022-2024 reveal a consistent peak in both hotspot counts and total BA during the August-September period, with 2023 exhibiting the most extreme fire intensity (Figure 14). This peak aligns perfectly with the previously analyzed maximums in $PM_{2.5}$, CO, and NO_2, as well as the minimal rainfall recorded in August 2023.

Spatial analysis using a 2° buffer from Pontianak's administrative boundary indicates that the majority of fire activity occurred in the peatland-dominated regions to the South and East. Given the low frequency of local fires within the city itself, these results confirm that the hazardous $PM_{2.5}$ levels in Pontianak are primarily driven by the regional transport of persistent smoke from surrounding peatland burning.

To evaluate the suitability of pollutant trajectories, wind field dynamics from ERA5 reanalysis were overlaid with active fire locations (Figure 15). During the peak event (12-14 August 2023), wind patterns displayed a consistent vertical structure from the surface (10 m) up to the lower atmosphere (100 m), dominated by stable Southeasterly flows (3 - 6 m/s). This uniformity confirms the dominance of the dry season background flow, effectively channeling smoke from fire sources.

The spatial distribution of BA around Pontianak further validates this transport mechanism. Analysis using incremental buffers up to 2° from the city center reveals that the vast majority of BA occurred in the peatland regions to the South and East (Figure 16). The intense BA observed in August 2023 (indicated by dark blue clusters) corresponds directly to the sustained clustered hotspots, reinforcing the argument that high urban $PM_{2.5}$ levels were driven by regional trans-boundary haze originating from intensive peat burning in these upwind areas.

4. CONCLUSIONS

This study confirms that 2023 was the most critical period for air quality in Pontianak, with CO, $PM_{2.5}$, PM_{10}, NO_2, and HC levels significantly higher than in 2022 or 2024. While inherent satellite limitations, such as signal saturation during extreme haze, lead to some underestimation under maximum pollution conditions, the HGBR framework effectively bridges the data gaps left by limited ground stations. Ultimately, these results provide a strong scientific foundation for the development of operational early warning systems tailored to fire-affected tropical environments. This framework serves as a necessary tool for proactive public health protection and data-driven haze mitigation. Future work should explore higher-resolution imagery and deep learning architectures to further enhance predictive accuracy for stakeholders in Indonesia.

5. ACKNOWLEDGEMENT

The authors would like to thank the National Research and Innovation Agency (BRIN), Jakarta, Indonesia and Environment Agency of Pontianak City, Pontianak, Indonesia for the support provided during this research.

REFERENCES

Ahmed, M. F., B. Rana, B. Halder, M. Pramanik, H. S. Shakir, and Z. M. Yaseen (2025). Assessing Atmospheric Pollution in Asian Major Cities Through Sentinel-5P and Google Earth Engine: A Remote Sensing Approach. *Theoretical and Applied Climatology*, **156**(9); 458

Arshad, N., N. Mazhar, and A. Ahmad (2025). Assessment of Air Quality Variations in Punjab, Pakistan, Using Sentinel-5P During COVID-19 Lockdowns. *Environmental Monitoring and Assessment*, **197**(12); 1328

Atkinson, A. C., M. Riani, and F. Torti (2016). Robust Methods for Heteroskedastic Regression. *Computational Statistics & Data Analysis*, **104**; 209–222

Aziis, D. M., A. Wirasatriya, and H. Setiyono (2025). Pengaruh El Nino Kuat 2023 Terhadap Variabilitas Suhu Permukaan Laut dan Curah Hujan di Laut Sawu. *Indonesian Journal of Oceanography*, **7**(1); 32–41. (in Indonesian)

Balsamo, G., A. Agusti-Panareda, C. Albergel, G. Arduini, A. Beljaars, J. Bidlot, E. Blyth, N. Bousserez, S. Boussetta, A. Brown, R. Buizza, C. Buontempo, F. Chevallier, M. Choulga, H. Cloke, M. F. Cronin, M. Dahoui, P. De Rosnay, P. A. Dirmeyer, and X. Zeng (2018). Satellite and In Situ Observations for Advancing Global Earth Surface Modelling: A Review. *Remote Sensing*, **10**(12); 2038

Bennouna, Y. S., V. E. Cachorro, D. Mateos, M. A. Burgos, C. Toledano, B. Torres, and A. M. De Frutos (2016). Long-Term Comparative Study of Columnar and Surface Mass Concentration Aerosol Properties in a Background Environment. *Atmospheric Environment*, **140**; 261–272

Berg, P., H. Feldmann, and H.-J. Panitz (2012). Bias Correction of High Resolution Regional Climate Model Data. *Journal of Hydrology*, **448–449**; 80–92

Binte Habib, A., M. G. R. Alam, and M. Z. Uddin (2025). AUNET (Attention-Based Unified Network): Leveraging Attention-Based N-BEATS for Enhanced Univariate Time Series Forecasting. *IEEE Access*, **13**; 95184–95217

Breiman, L. (2001). Random Forests. *Machine Learning*, **45**(1); 5–32

Burnett, R., H. Chen, M. Szyszkowicz, N. Fann, B. Hubbell, C. A. Pope, J. S. Apte, M. Brauer, A. Cohen, S. Weichenthal, J. Coggins, Q. Di, B. Brunekreef, J. Frostad, S. S. Lim, H. Kan, K. D. Walker, G. D. Thurston, R. B. Hayes, and J. V. Spadaro (2018). Global Estimates of Mortality Associated with Long-Term Exposure to Outdoor Fine Particulate Matter. *Proceedings of the National Academy of Sciences*, **115**(38); 9592–9597

Chen, J., Y. Liu, M. Zhang, and Y. Peng (2016). New Understanding and Quantification of the Regime Dependence of Aerosol–Cloud Interaction for Studying Aerosol Indirect Effects. *Geophysical Research Letters*, **43**(4); 1780–1787

Coelho, C. A. S., C. A. T. Ferro, D. B. Stephenson, and D. J. Steinskog (2008). Methods for Exploring Spatial and Temporal Variability of Extreme Events in Climate Data. *Journal of Climate*, **21**(10); 2072–2092

Crippa, P., S. Castruccio, S. Archer-Nicholls, G. B. Lebron, M. Kuwata, A. Thota, S. Sumin, E. Butt, C. Wiedinmyer, and D. V. Spracklen (2016). Population Exposure to Hazardous Air Quality Due to the 2015 Fires in Equatorial Asia. *Scientific Reports*, **6**(1); 37074

Doreswamy, K. S. H., Y. Km, and I. Gad (2020). Forecasting Air Pollution Particulate Matter (PM2.5) Using Machine Learning Regression Models. *Procedia Computer Science*, **171**; 2057–2066

Ghafarian, F., R. Wieland, D. Lüttschwager, and C. Nendel (2022). Application of Extreme Gradient Boosting and Shapley Additive Explanations to Predict Temperature Regimes Inside Forests from Standard Open-Field Meteorological Data. *Environmental Modelling & Software*, **156**; 105466

Guo, M., H. Zhang, and P. Xia (2020). A Method for Predicting Short-Time Changes in Fine Particulate Matter ($PM_{2.5}$) Mass Concentration Based on the Global Navigation Satellite System Zenith Tropospheric Delay. *Meteorological Applications*, **27**(1); e1866

Guryanov, A. (2019). Histogram-Based Algorithm for Building Gradient Boosting Ensembles of Piecewise Linear Decision Trees. In W. M. P. Van Der Aalst, V. Batagelj, D. I. Ignatov, M. Khachay, V. Kuskova, A. Kutuzov, S. O. Kuznetsov, I. A. Lomazova, N. Loukachevitch, A. Napoli, P. M. Pardalos, M. Pelillo, A. V. Savchenko, and E. Tutubalina, editors, *Analysis of Images, Social Networks and Texts*, volume 11832. Springer International Publishing, pages 39–50

Gustafson, W. I. and S. Yu (2012). Generalized Approach for Using Unbiased Symmetric Metrics with Negative Values: Normalized Mean Bias Factor and Normalized Mean Absolute Error Factor. *Atmospheric Science Letters*, **13**(4); 262–267

Handschuh, J., T. Erbertseder, and F. Baier (2024). On the Added Value of Satellite AOD for the Investigation of Ground-Level PM2.5 Variability. *Atmospheric Environment*, **331**; 120601

Huang, X. and G. Rein (2014). Smouldering Combustion of Peat in Wildfires: Inverse Modelling of the Drying and the Thermal and Oxidative Decomposition Kinetics. *Combustion and Flame*, **161**(6); 1633–1644

Johnston, F. H., S. B. Henderson, Y. Chen, J. T. Randerson, M. Marlier, R. S. DeFries, P. Kinney, D. M. J. S. Bowman, and M. Brauer (2012). Estimated Global Mortality Attributable to Smoke from Landscape Fires. *Environmental Health Perspectives*, **120**(5); 695–701

Karim, M., S. Tomar, S. K. Shah, and T. P. Singh (2025). Analyzing and Predicting PM_{10} Using Remote Sensing and Machine Learning: A Case Study of Delhi, India. *Discover Applied Sciences*, **7**(11); 1291

Kong, L., J. Xin, W. Zhang, and Y. Wang (2016). The Empirical Correlations Between $PM_{2.5}$, PM_{10} and AOD in the Beijing Metropolitan Region and the $PM_{2.5}$, PM_{10} Distributions Retrieved by MODIS. *Environmental Pollution*, **216**; 350–360

Ma, P., F. Tao, L. Gao, S. Leng, K. Yang, and T. Zhou (2022). Retrieval of Fine-Grained $PM_{2.5}$ Spatiotemporal Resolution Based on Multiple Machine Learning Models. *Remote Sensing*, **14**(3); 599

Marlier, M. E., R. S. DeFries, P. S. Kim, D. L. A. Gaveau, S. N. Koplitz, D. J. Jacob, L. J. Mickley, B. A. Margono, and S. S. Myers (2015). Regional Air Quality Impacts of Future Fire Emissions in Sumatra and Kalimantan. *Environmental Research Letters*, **10**(5); 054010

Miah, M. T., R. Raiyan, R. A. Mishu, M. R. Hasan, R. Islam, P. K. Jodder, and K. R. Rahaman (2025). Decoding Climatic Variability and Ecosystem Impact: Integrating Satellite-Derived Data and Geospatial Techniques for Holistic Air Quality Assessment in Nova Scotia. *Theoretical and Applied Climatology*, **156**(10); 523

Murray, C. J. L., A. Y. Aravkin, P. Zheng, C. Abbafati, K. M. Abbas, M. Abbasi-Kangevari, F. Abd-Allah, A. Abdelalim, M. Abdollahi, I. Abdollahpour, K. H. Abegaz, H. Abolhassani, V. Aboyans, L. G. Abreu, M. R. M. Abrigo, A. Abualhasan, L. J. Abu-Raddad, A. I. Abushouk, M. Adabi, and S. S. Lim (2020). Global Burden of 87 Risk Factors in 204 Countries and Territories, 1990–2019: A Systematic Analysis for the Global Burden of Disease Study 2019. *The Lancet*, **396**(10258); 1223–1249

Pope, C. A. and D. W. Dockery (2006). Health Effects of Fine Particulate Air Pollution: Lines That Connect. *Journal of the Air & Waste Management Association*, **56**(6); 709–742

Ravish, P., S. Chaudhry, and A. Sharma (2025). Impact of Different Crop Residue Burning Activities on Seasonal Variation in Ambient Air Quality. *Discover Atmosphere*, **3**(1); 22

Reid, J. S., E. J. Hyer, R. S. Johnson, B. N. Holben, R. J. Yokelson, J. Zhang, J. R. Campbell, S. A. Christopher, L. Di Girolamo, L. Giglio, R. E. Holz, C. Kearney, J. Miettinen, E. A. Reid, F. J. Turk, J. Wang, P. Xian, G. Zhao, R. Balasubramanian, and S. C. Liew (2013). Observing and Understanding the Southeast Asian Aerosol System by Remote Sensing: An Initial Review and Analysis for the Seven Southeast Asian Studies (7SEAS) Program. *Atmospheric Research*, **122**; 403–468

Shofiana, D. A., M. Caniadi, R. Sholehurrohman, and Aristoteles (2025). Decision Tree Algorithms in Water Quality Classification: A Comparative Study of Random Forest, XGBoost, and C5.0. *Science and Technology Indonesia*, **10**(4); 999–1011

Stavros, E. N., D. McKenzie, and N. Larkin (2014). The Climate-Wildfire-Air Quality System: Interactions and Feedbacks Across Spatial and Temporal Scales. *WIREs Climate Change*, **5**(6); 719–733

Subhi Malallah, H. and M. Bahjat Abdulrazzaq (2023). Web-Based Agricultural Management Products for Marketing System: Survey. *Academic Journal of Nawroz University*, **12**(2); 49–62

Uyanık, G. K. and N. Güler (2013). A Study on Multiple Linear Regression Analysis. *Procedia - Social and Behavioral Sciences*, **106**; 234–240

Van Der Werf, G. R., J. T. Randerson, L. Giglio, T. T. Van Leeuwen, Y. Chen, B. M. Rogers, M. Mu, M. J. E. Van Marle, D. C. Morton, G. J. Collatz, R. J. Yokelson, and P. S. Kasibhatla (2017). Global Fire Emissions Estimates During 1997–2016. *Earth System Science Data*, **9**(2); 697–

720

Velastegui-Montoya, A., N. Montalván-Burbano, P. Carrión-Mero, H. Rivera-Torres, L. Sadeck, and M. Adami (2023). Google Earth Engine: A Global Analysis and Future Trends. *Remote Sensing*, **15**(14); 3675

Vetrita, Y., I. Albar, I. Santoso, I. Prasasti, T. Kartika, A. B. Usman, A. Tosiani, D. Haryanto, Endrawati, E. Famurianty, K. Ulfa, and J. Purwanto (2025a). Monthly Mapping of Indonesia's Burned Areas: Implementation, History, Techniques, and Future Directions. *International Journal of Remote Sensing*, **46**(2); 636–660

Vetrita, Y., K. Diwyacitta, K. M. Sukarno, I. Albar, A. B. Usman, R. P. Ritonga, I. Santoso, A. I. Lestari, T. Kartika, D. A. Novresiandi, I. Prasasti, K. Ulfa, N. Novita, S. E. Siwi, S. Augusto, E. T. Prakoso, K. I. N. Rahmi, U. C. Nugroho, J. Widodo, and M. A. Cochrane (2025b). Evaluating the Capabilities of High-Resolution PlanetScope and Sentinel-2 Images for Mapping Burned Area and Vegetation Regrowth in Indonesia's Savannas. *International Journal of Remote Sensing*, **46**(18); 6803–6825

Xu, X., T. Tong, W. Zhang, and L. Meng (2020). Fine-Grained Prediction of $PM_{2.5}$ Concentration Based on Multisource Data and Deep Learning. *Atmospheric Pollution Research*, **11**(10); 1728–1737

Yin, L., C. Jiang, X. Wen, C. Du, W. Zhong, Z. Feng, Y. Long, and Y. Ma (2019). Microplastic Pollution in Surface Water of Urban Lakes in Changsha, China. *International Journal of Environmental Research and Public Health*, **16**(9); 1650

Yulianti, Y., R. Rupita, S. E. Rahmaniah, S. Syarmiati, and S. Sudirman (2024). Impact of Forest and Land Fires on Environmental Pollution and Public Health in Sungai Raya Sub-District, Kubu Raya District. *International Journal of Multidisciplinary Approach Research and Science*, **2**(02); 787–800

Zaib, S., J. Lu, and M. Bilal (2022). Spatio-Temporal Characteristics of Air Quality Index (AQI) over Northwest China. *Atmosphere*, **13**(3); 375

Zhao, Q., L. Yu, X. Li, D. Peng, Y. Zhang, and P. Gong (2021). Progress and Trends in the Application of Google Earth and Google Earth Engine. *Remote Sensing*, **13**(18); 3778